Submitted to the Journal of Intelligent Material Systems and Structures
May 30, 2011

Rheology and microstructural evolution in pressure-driven flow of a magnetorheological fluid with strong particle-wall interactions

Murat Ocalan[1,2], *Gareth H. McKinley*[1]

[1]Hatsopoulos Microfluids Laboratory, Department of Mechanical Engineering,
Massachusetts Institute of Technology, 77 Massachusetts Ave. Cambridge, Mass. 02139

[2]Schlumberger-Doll Research, 1 Hampshire St. Cambridge, Mass. 02139

Abstract

The interaction between magnetorheological (MR) fluid particles and the walls of the device that retain the fluid is critical as this interaction provides the means for coupling the physical device to the field-controllable properties of the fluid. This interaction is often enhanced in actuators by the use of ferromagnetic walls which generate an attractive force on the particles in the field-on state. In this paper, the aggregation dynamics of MR fluid particles and the evolution of the microstructure in pressure-driven flow through ferromagnetic channels are studied using custom-fabricated microfluidic devices with ferromagnetic side walls. The aggregation of the particles and the time-dependent evolution in the microstructure is studied in rectilinear, expansion and contraction channel geometries. These observations help identify methods for improving MR actuator design and performance.

1. Introduction

Microscopy based studies into the microstructural evolution of field responsive fluids such as electrorheological (ER) and magnetorheological (MR) fluids have provided significant insight into the processes that result in their controllable bulk properties. The focus of these studies has been in the areas of chain deformation and breakup (Klingenberg and Zukoski, 1990) and in particle aggregation & disaggregation (Shulman et al., 1986, Fermigier and Gast, 1992, Melle et al., 2003, Dominguez-Garcia et al., 2005, Deshmukh, 2007). Quantitative understanding of the bulk rheological properties of these so-called 'smart' fluids, such as field-dependent yield stress, viscoelastic modulus and material response time, is intimately linked to these microstructural processes.

The dynamics and extent of local aggregation phenomena in MR fluids is governed by the dimensionless ratios of the magnetic forces to the other forces acting on particles including Brownian forces (Fermigier and Gast, 1992) and hydrodynamic forces (Melle et al., 2003, Deshmukh, 2007). The relative importance of these dimensionless parameters depends on the specific flow regime of interest.

It is important to distinguish the origins of the magnetic force so that we can understand the physical mechanisms governing the dynamics of aggregation. By making the uniform magnetization approximation, the magnetic force on a spherical particle can be treated as the force on a magnetic dipole of strength $\mathbf{m} = V\mathbf{M}_p$, where V is the volume of the particle and $\mathbf{M}_p$ is the magnetization (Zahn, 1987, Sect. 5-5-1). This approximation is exact in two limits

(Klingenberg et al., 2007): (1) When the particle has reached saturation magnetization, $M_p = M_S$, and 2) When the particle is isolated in a uniform magnetic field H, for which

$$m = VM_p = 4\pi a^3 \frac{\chi_m}{\chi_m + 3} H, \tag{1}$$

where χ_m is the magnetic susceptibility of the particle (Zahn, 1987, Sect. 5-7-2).

A magnetic force on the dipole only exists in an inhomogeneous field (for which $\nabla \mathbf{H} \neq 0$) and is determined by:

$$\mathbf{f}_{mag} = \mu_0 \mathbf{m} \cdot \nabla \mathbf{H}, \tag{2}$$

where μ_0 is the magnetic permeability of free space. The magnetic force generated between two particles placed in a homogeneous field can be viewed as arising from the distorted field lines of each magnetically susceptible particle. This interparticle force for the case of two spherical particles in contact is (Klingenberg et al., 2007):

$$f_{int} = \frac{\pi}{6} \mu_0 a^2 {M_p}^2, \tag{3}$$

and varies quadratically with magnetization. The challenge is to understand how such pairwise interactions between two particles are related to the overall properties of a dense suspension of MR-active particles which along the field lines form chained structures. Time-resolved microscopic observations under both equilibrium and flowing conditions are essential to make progress.

The evolution in microstructure of a quiescent MR suspension was studied by Fermigier and Gast (1992). In the absence of background flow, the aggregation and disaggregation phenomena was shown to be governed solely by the dimensionless ratio of the interparticle magnetic force to the Brownian force

$$\lambda = \frac{f_{int}}{f_B} = \frac{\pi \mu_0 a^3 M_P{}^2}{6 k_B T}. \tag{4}$$

Here, we have used the Brownian force scale, $f_B \sim k_B T / a$ (Sharma et al., 2009) where k_B is the Boltzmann constant and T is the absolute temperature.

In the presence of hydrodynamic forces additional dimensionless parameters are important. At the length scale of the individual particle, the Reynolds number is often small and the hydrodynamic force on the particle can be evaluated using the Stokes drag formula $f_d = 6\pi\eta a V$, where η_0 is the matrix viscosity. In a simple shear flow, the local velocity in this relation is $V = \dot{\gamma} a$ where $\dot{\gamma}$ is the shear rate. The dimensionless ratio of the magnetic force to the hydrodynamic force results in the Mason number (Marshall et al., 1989 (for equivalent problem in ER fluids), Klingenberg et al., 2007)

$$Mn = \frac{f_d}{f_{int}} = \frac{36 \eta_0 \dot{\gamma}}{\mu_0 M_P{}^2}. \tag{5}$$

Studies conducted using rotating magnetic fields (Melle et al., 2003) and pressure-driven flow in microfluidic channels (Haghgooie, 2006, Deshmukh, 2007) showed that in homogeneous magnetic fields, the aggregation dynamics of magnetically-susceptible particles in the presence of hydrodynamic forces are governed by the Mason number.

If the applied field is spatially inhomogeneous, the magnetic force on the particles is caused not only by the perturbation resulting from other neighboring particles but also by the background field gradients. We can estimate this magnetophoretic force by approximating the field to be locally uniform at the length scale of the particle, and therefore inserting Equation (1) into Equation (2) :

$$\mathbf{f}_{mag} = \mu_0 \left(\frac{4}{3} \pi a^3 \right) \mathbf{M}_p \cdot \nabla \mathbf{H} = 4\pi \mu_0 a^3 \beta H \left(\nabla H \right) \tag{6}$$

where the effective susceptibility, $\beta = \chi_m / (\chi_m + 3)$. To obtain the second equality, we made use of the vector identity $\mathbf{H} \cdot \nabla \mathbf{H} = H \nabla H - \mathbf{H} \times (\nabla \times \mathbf{H})$ and the magnetostatic Ampere's Law in the absence of free current $(\nabla \times \mathbf{H} = 0)$ (Rosensweig, 1979). Comparing this force to Stokes drag, we find another dimensionless parameter:

$$\Psi = \frac{f_{mag}}{f_d} = \frac{2\mu_0 a^2 \beta H}{3\eta_0 V_b} \frac{\partial H}{\partial x}, \tag{7}$$

where the background flow velocity, V_b, is in the x-direction. Since we are considering the balance between the magnetophoretic force and the hydrodynamic force acting on a particle, the velocity scale V_b in this case is left in terms of the local velocity of the background flow as opposed to the shear rate that is incorporated in the definition of the Mason number. In other words, magnetostatic forces can affect particle motion even in uniform translational flows of an MR suspension for which $\mathbf{V} = V_b \mathbf{e}_x$ if the field is inhomogeneous.

Kuzhir and coworkers (2005) studied the flow of non-magnetic particles suspended in a ferrofluid (a magnetic colloidal system) in non-uniform magnetic fields. An important dimensionless parameter identified in their two-phase flow model was the quantity $A = (9\eta_0 x_{\max} v) \big/ \left(2a^2 \mu_0 M_S H_{\max}\right)$ where $H_{\max}$ and $x_{\max}$ are the relevant scales for magnetic field intensity and distance of field decay. This quantity is related to Equation (7) and in fact we can see that $A \approx \Psi^{-1}$ by describing the saturation magnetization in terms of the local field and effective susceptibility, $M_S = 3\beta H$ and recognizing that the inhomogeneous gradient $(\partial H / \partial x) \approx (H_{\max} / x_{\max})$. Microstructure and aggregation phenomena in non-uniform magnetic fields from a microscopic perspective, however, have not been investigated for either suspension of non-magnetic particles in ferrofluids or MR fluids.

In order to quantify the relative magnitude of the forces in an MR suspension, it is necessary to design and construct flow channels that allow simultaneous observation of microstructure evolutions as well as macroscopic quantities such as the field-dependent yield stress or pressure drop. In the present study we describe a fabrication process that enables us to construct microfluidic channels in which we can simultaneously observe the formation in fluid flow as well as the resulting changes in the hydrodynamic resistance exerted by the MR fluid as an external magnetic field is applied.

The interaction between the individual MR fluid particles and the surfaces that retain the fluid is extremely important because it can limit the extent of momentum transfer to/from the fluid through the liquid/solid interface. Deshmukh (2007) used high-speed video microscopy to investigate the aggregation phenomena in pressure-driven flow of MR fluids in smooth glass and

poly-dimethylsiloxane (PDMS) microfluidic channels. It was found that, in the absence of a strong particle-wall interaction there is significant slip of the particles and field-induced aggregates along channel walls. The consequences of this on the macroscopic pressure drop were not measured, but any wall-slip is expected to reduce the resulting shear stress exerted by the fluid on the wall. Particle-wall interaction is commonly enhanced in applications and in rheometric studies by controlling the surface roughness and selecting ferromagnetic channel materials. These enhancement methods were demonstrated to increase the field-dependent shear stress exerted by MR fluids in the bulk rheological study conducted by Laun and coworkers (2011). In MR fluid applications, ferromagnetic channel walls are often utilized (Jolly et al., 1999, Herr and Wilkenfeld, 2003) and studies of chain formation and flow adjacent to ferromagnetic walls therefore has more engineering significance.

In the present study, we investigate the microstructural evolution of MR fluids in microchannels with ferromagnetic side walls. The strong interaction between the MR fluid particles and the channel walls provides a means to study aggregation and flow phenomena in these field-responsive fluids with boundary conditions replicating those realized in actuators. We also explore the flow of MR fluid through more complex channels such as contraction and expansion geometries that lead to inhomogeneous magnetic fields induced by the ferromagnetic channel walls.

2. Experimental methods

The rectilinear channels used in this study were manufactured by adhering two ferromagnetic sheets with a separation of $h = 1.2mm$ between two glass microscope cover slips

as illustrated in Figure 1b. In order to generate a uniform field in the flow path, additional external ferromagnetic plates were assembled on each side of the microfluidic channel. The metallic components were manufactured from sheets of low carbon steel (1008/1010 carbon steel for $0.3mm$ thick pieces and CS Type B for $1mm$ pieces) using hydraulic shears and deburred using sandpaper.

The benefits provided by the external plates can be understood from the two dimensional finite element model, which was implemented in Comsol Multiphysics®. The model is solved for the magnetic vector potential in the out-of plane directions, A_z . In the absence of free current, the governing equation reduces to a scalar Laplace's equation $(\nabla^2 A_z = 0)$. The relative magnetic permeability in the model is unity except for the ferromagnetic sheets where it is $\mu_r = 10^3$. The boundary conditions, which are set far from the geometrical features, are defined as constant vector potential conditions on the top and the bottom surfaces, and perpendicular field conditions on the side walls. These conditions generate a uniform applied field far from the channel features. The results of the first simulation, presented in Figure 2a, show that in the absence of the external plates the field uniformity is very poor with a strong gradient towards the sharp corners of the ferromagnetic channel walls. MR fluid flowing in this type of channel would experience an undesirable magnetophoretic force towards the channel walls. In the second simulation (Figure 2b) the external plates located above the glass cover slips are also included. In this case the field uniformity is significantly improved with fringing fields shifted away from the microfluidic flow channel.

The entire assembly is designed to be placed on the stage of an inverted microscope (Nikon TE-2000S) and viewed with microscope objectives 2X 0.06NA objective and a

monochromatic CCD camera (Matrix Vision BlueFOX). The depth of field of this imaging system is $240\mu m$ and the image resolution is $3.4\,\mu m/pixel$.

During the flow visualization experiments, the channel is placed between the poles of a custom built electromagnet as illustrated in Figure 1a. The field applied by the magnet was calibrated using a Gauss probe placed in the mid-point between the poles of the magnet. The flux density at this point was found to be $B_M = 22mT$ at a DC coil potential drop $V_C = 25V$. Because of the dimensional constraints of the probe, it was not possible to conduct this measurement within the microchannels after assembly. The amplification of the field in the narrow gap, caused by the channel walls was estimated using the results of the finite element model, as presented in Figure 2b. The magnetic flux density in the channel is $B_C = 6B_M$.

Prior to each experiment the ferromagnetic walls of the flow channel was demagnetized using a time-varying magnetic field in the form

$$B_C(t) = B_0 \cos(2\pi f t)\, e^{-\alpha t}. \tag{8}$$

Here B_0 is the initial amplitude of the signal which is normally set as the largest field applied since the preceding demagnetization cycle. The constants f and α are normally selected in the ranges $1-10Hz$ and $0.3-1s^{-1}$ respectively.

The MR fluid used in the experiments was prepared by suspending 1% v/v carbonyl iron particles (BASF® CR-grade) with a mean diameter of $7\mu m$ in a mixture of PDMS fluid and 10% w/w surfactant (Gelest™ DMS-T31 and DMS-S31 respectively, both fluids with viscosity $\eta_0 = 1Pa.s$). The surfactant was incorporated in the fluid to promote the dispersion of the

particles in the matrix fluid. The preparation procedure of the fluid was similar to that of Deshmukh (2007). The fluid was first mixed in an ultrasonic bath for 30 minutes followed by a cycle in a conditioning mixer (Thinky® AR-310). The cycle consisted of 2 minutes of mixing, 1 minute of degassing and 1 minute of mixing. These steps were found to repeatably prepare a well dispersed sample without the presence of air inclusions. The fluid was pumped through the channel using a syringe pump (Harvard Apparatus® PHD 4400) with a constant flow rate, Q. The pressure drop across the channel was measured with a differential pressure transducer (Honeywell 26PCBFA6D) with a measurement range of $34kPa$.

The resulting 2D video images were analyzed with a cluster identification algorithm in order to quantify the observations made on the aggregation phenomena. These images are a 2D projection of the 3D structure across the $0.3mm$ height of the channel. Because of the strong particle-wall interactions, under applied fields, the particle density near the walls is relatively high, causing the particle phase to appear as the continuous phase in most of these images (see Figure 3). The cluster identification algorithm was used to seek clusters of voids instead of particle aggregates. Following the methodology of Deshmukh (2007), grayscale images captured from the video camera were binarized using a thresholding algorithm. The level of thresholding was selected using the minimum histogram method (Russ, 2002). We can understand the utility of this method by realizing that the original image is made up of a bimodal distribution of dark and bright pixels, as shown in Figure 3c. The appropriate value for thresholding is located in between the peaks in the histogram. Exploratory calculations showed that the exact value chosen within this valley does not materially affect the results of this analysis because the number of clusters is so much smaller than the total number of pixels. The black-and-white image obtained

with this method was processed with a cluster identification algorithm using the Matlab® Image Analysis Toolbox. The output of this algorithm is illustrated in Figure 3b.

3. Results

Images recorded during a typical straight channel experiment are presented in Figure 4. In a demagnetized channel, the flow of the MR fluid occurs without aggregation of the particles. When the field is applied, the aggregates that form can be categorized into three groups by the number of channel walls the aggregate is in contact with: 0 (free-flowing clusters), 1 or 2 (channel-spanning). The aggregates that belong to the latter group come to a complete stop within the flow channel under the influence of strong particle-wall interactions. The deformed shape of these chains arises from the local balance of hydrodynamic and magnetic dipolar force acting on the particle. The aggregates contacting only one of the channels also come to a stop at the channel wall; however, they continue to rotate under the influence of the flow until they contact another aggregate or until the magnetic torque on the chained aggregate becomes equal to the hydrodynamic torque. Finally, the aggregates that do not have any contact with the channel walls flow continuously under the influence of the hydrodynamic forces; however, many eventually merge with a wall-contacting or channel-spanning aggregate and stop flowing. The matrix phase continues to flow continuously through the channel and there is thus a relative "slip" between the particle phase and the suspending solvent, Upon removal of the magnetic field, most of the particles in the channel freely flow once more. However, the particles close to the walls remain adhered to the interface (Figure 4c), forming a particle-enriched layer on both sides of the channel. These layers contribute to the residual extra pressure drop ΔP_{rem} across the

channel as seen in Figure 5. This extra pressure drop can be thought of as a reduction of the channel dimensions caused by the presence of the particle-rich layers. In a 2D flow approximation with $w \gg h$, the additional pressure drop can be described in terms of an effective channel width

$$w_{eff}^{w \gg h} = w\left(1 + \frac{\Delta P_{rem}}{\Delta P_0}\right)^{-1} \tag{9}$$

where ΔP_0 is the pressure drop in the channel prior to the application of the magnetic field. For common MR fluid valve applications, however, the aspect ratio of the channel width and height are reversed with $w \ll h$ (noting that the field is applied along the width of the channel w). In this case, the flow can again be approximated as 2D, however now the effective width is

$$w_{eff}^{w \ll h} = w\left(1 + \frac{\Delta P_{rem}}{\Delta P_0}\right)^{-1/3} \tag{10}$$

When a demagnetizing field protocol is applied (Equation (8)), the remnant field in the channel walls is effectively eliminated and all particles and aggregates flow out of the channel under the action of hydrodynamic stresses. The pressure drop across the channel also returns to its original value at the end of the demagnetizing step.

The aggregate structures formed over a wide range of Mason numbers are presented in Figure 6. The magnetic field is applied rapidly on a demagnetized flow channel and the images shown are recorded when the field-induced structure formation in the flow has reached a steady state. There is a general trend of increase in the aggregated structure with decreasing Mn, which can be quantitatively identified by the cluster detection algorithm, as presented in the plots of the

void extents shown in Figure 7. For this concentration of MR particles we observe a maximum in the void spacing at $Mn = 1.6 \times 10^{-3}$. This maximum arises because at this Mason number, large clusters develop from discrete chains in the fluid colliding and merging with clusters already attached to the wall. As the field strength increases further, the majority of the particles form channel-spanning chains and cease flowing entirely before aggregation with other chains can occur.

The aggregation and flow phenomena in the contraction and expansion geometries were also studied under a low-frequency $(0.1Hz)$ periodic applied field. The field was constantly on for the first half of the cycle followed by a demagnetizing field $(f = 10Hz, \alpha = 0.44$ in Eq. (1)$)$ for the second half. With this selection of parameters, the decay in the demagnetizing field is rapid enough that the field is effectively removed entirely for the last 40% of the cycle. A sequence of images obtained in these flow conditions are illustrated in Figure 8. The aggregation in the inhomogeneous field sections outside the rectilinear channel shows a preferred direction aligned with the local field. Furthermore, an increase or a decrease in the convective velocity of the particle clusters is also observed because of the magnetic field gradients in these converging/diverging flows. The magnitude of this magnetophoretic response can be evaluated using the dimensionless parameter Ψ defined in Equation (7). For these flow geometry the field gradient can be approximated by $|\partial H/\partial x| \approx B_C/(\mu_0 w)$. The effective susceptibility, β was taken to be unity, in accordance with the infinitely permeable particle approximation. Reversal in flow direction of the particulate phase was also observed in the expansion channel under a high magnetic field $B_C = 0.1mT$ and low flow rate $Q = 10\,\mu l/min$ corresponding to $\Psi \approx -0.12$. This reversal can be observed by following the particles located in the circled region in Figure 8b.

When the field is turned on these particles not only form an aggregate but also flow back into the narrow channel under the influence of magnetophoretic forces.

4. Conclusions and discussion

We have described a unique microfluidic channel setup with ferromagnetic walls that enables flow of an MR fluid with strong particle-wall interaction. The forces caused by this strong particle-wall interaction were demonstrated to be large enough to effectively eliminate the slip of the particulate phase against the channel walls. Under these boundary conditions the aggregation phenomena in rectilinear flow channels were studied by varying the Mason number.

Under the influence of an externally applied magnetic field, the particles in the fluid from anisotropic aggregates with the average size of these clusters a function of the Mason number. At low Mason numbers the aggregate size increases with this parameter; however the aggregate size reaches a maximum at a critical Mason number then shows a decreasing trend. This was linked to a larger time-scale aggregation phenomena, which occurs as free-flowing aggregates collide and merge with wall-attached aggregates. At higher fields (lower *Mn*), this aggregation process loses its importance, as more of the particles immediately form channel spanning aggregates with the application of the magnetic field, stop flowing, and therefore stop aggregating.

The magnetic field gradient in the entry and exit regions of the converging/diverging flow channels can generate additional magnetophoretic forces on the particles that can be significant as compared with the hydrodynamic force. The relative importance of the magnetophoretic force in relation to the hydrodynamic force can be determined by the dimensionless parameter Ψ given in Equation (7). For flows with $\Psi \gg -0.1$, the

magnetophoretic force can drive secondary flows. With the combination of the magnetophoretic force in the entry & exit regions and the no-slip condition on the particulate phase, a slow increase in particle volume fraction in the converging/diverging channels was observed in experiments with Ψ of high magnitude.

By direct imaging the steady flow of an MR suspension in an inhomogeneous magnetic field it is clear that a simple isotropic continuum model such as a Bingham or Casson model with a field-dependent yield stress $\tau_y(B)$ will be insufficient for describing the dynamics of MR suspensions in real devices. An alternate approach that we are currently exploring is to self-consistently incorporate the anisotropic and field-dependent particle level stresses in a two-fluid suspension balance model of the type considered by Nott and Brady (1994), and Fan and coworkers (2000).

An additional benefit in utilizing these types of models is their treatment of the multi-body effects in the evaluation of the hydrodynamic and magnetic forces in a suspension. For defining Ψ we analyzed the micromechanics of isolated particles in order to obtain correlations for the forces acting on an MR fluid particle. In doing so we neglected the multi-body effects, which is consistent with the approach used to develop other dimensionless parameters such as Mn and λ. Using a continuum description of the MR suspension, it may be possible to describe the forces in the MR suspension with a higher degree of accuracy which can allow quantitative analytical and computational studies of the complex two-phase flows in inhomogeneous fields.

References

Deshmukh SS (2007) *Development, characterization and applications of magnetorheological fluid based 'smart' materials on the macro-to-micro scale*. PhD Thesis, Massachusetts Institute of Technology, Dept. of Mech. Eng.

Dominguez-Garcia P, Melle S, Calderon OG, Rubio MA (2005) Doublet dynamics of magnetizable particles under frequency modulated rotating fields. *Colloid Surface A* 270: 270-276. DOI 10.1016/j.colsurfa.2005.06.012

Fan XJ, Phan-Thien N, Zheng R (2000) Simulation of fibre suspension flow with shear-induced migration. *J Non-Newton Fluid* 90: 47-63

Fermigier M, Gast AP (1992) Structure evolution in a paramagnetic latex suspension. *J Colloid Interf Sci* 154: 522-539

Haghgooie R (2006) *Structure and dynamics of magnetorheological fluids confined in microfluidic devices*. PhD Thesis, Massachusetts Institute of Technology, Dept. of Chem. Eng.

Herr H, Wilkenfeld A (2003) User-adaptive control of a magnetorheological prosthetic knee. *Ind Robot* 30: 42-55. DOI 10.1108/01439910310457706

Jolly MR, Bender JW, Carlson JD (1999) Properties and applications of commercial magnetorheological fluids. *J Intel Mat Syst Str* 10: 5-13

Klingenberg DJ, Ulicny JC, Golden MA (2007) Mason numbers for magnetorheology. *J Rheol* 51: 883-893. DOI 10.1122/1.2764089

Klingenberg DJ, Zukoski CF (1990) Studies on the Steady-Shear Behavior of Electrorheological Suspensions. *Langmuir* 6: 15-24

Kuzhir P, Bossis G, Bashtovoi V, Vekas L (2005) Capillary flow of a suspension of non-magnetic particles in a ferrofluid under highly non-uniform magnetic field. *Int J Multiphase Flow* 31: 201-221. DOI 10.1016/j.ijmultiphaseflow.2004.09.006

Laun HM, Gabriel C, Kieburg C (2011) Wall material and roughness effects on transmittable shear stresses of magnetorheological fluids in plate-plate magnetorheometry. *Rheol Acta* 50: 141-157. DOI 10.1007/s00397-011-0531-8

Marshall L, Zukoski CF, Goodwin JW (1989) Effects of electric-fields on the rheology of non-aqueous concentrated suspensions. *J Chem Soc Farad T 1* 85: 2785-2795

Melle S, Calderon OG, Rubio MA, Fuller GG (2003) Microstructure evolution in magnetorheological suspensions governed by Mason number. *Phys Rev E* 68. DOI 10.1103/PhysRevE.68.041503

Nott PR, Brady JF (1994) Pressure-Driven Flow of Suspensions - Simulation and Theory. *J Fluid Mech* 275: 157-199

Rosensweig RE (1979) Magnetic stabilization of the state of uniform fluidization. *Ind Eng Chem Fund* 18: 260-269

Russ JC (2002) *The Image Processing Handbook*. CRC Press, Boca Raton

Sharma V, Park K, Srinivasarao M (2009) Colloidal dispersion of gold nanorods: Historical background, optical properties, seed-mediated synthesis, shape separation and self-assembly. *Mater Sci Eng R* 65: 1-38. DOI 10.1016/j.mser.2009.02.002

Shulman ZP, Kordonsky VI, Zaltsgendler EA, Prokhorov IV, Khusid BM, Demchuk SA (1986) Structure, physical-properties and dynamics of magnetorheological suspensions. *Int J Multiphase Flow* 12: 935-955

Zahn M (1987) *Electromagnetic Field Theory : A Problem Solving Approach*. R.F. Krieger, Malabar, Fla.

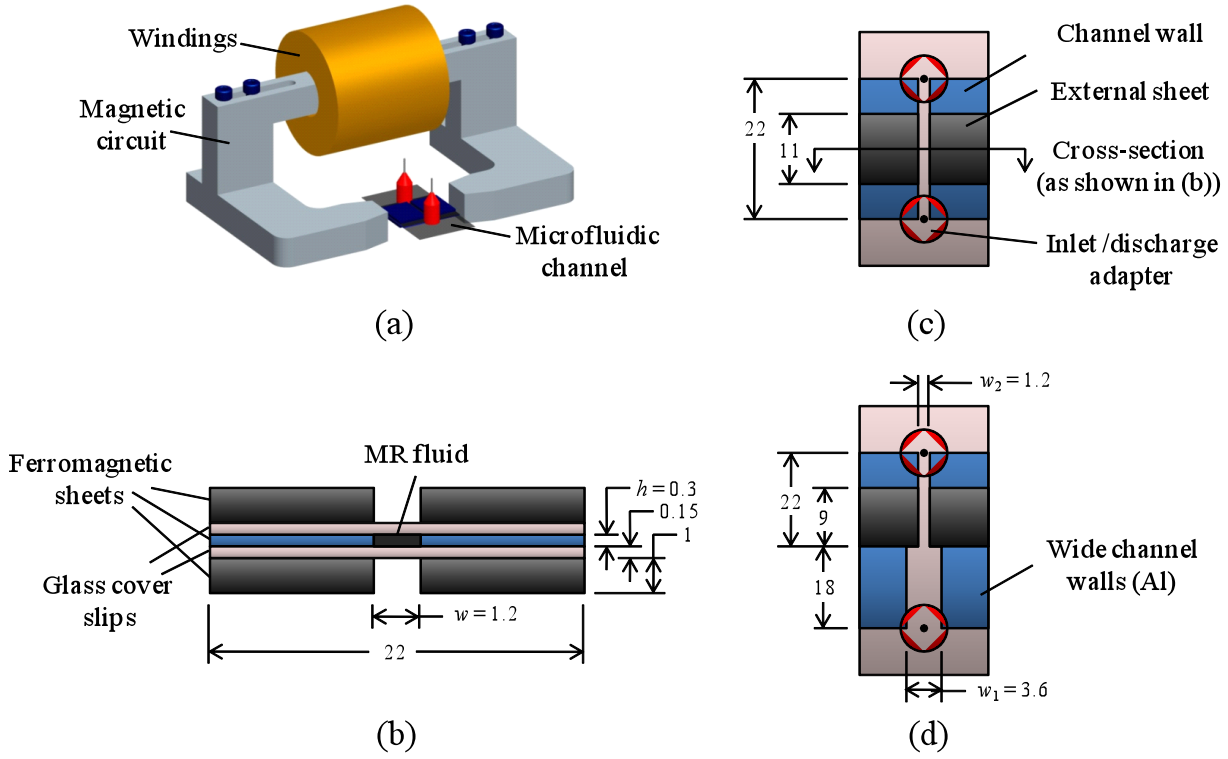

Figure 1: Experimental setup and microchannel channel construction. (a) The applied magnetic field is generated using a custom-built electromagnet. (b) Cross-sectional view of the microchannel in the flow direction. The channels used in this study are manufactured using a multilayered sandwich construction to provide a thin plane of fluid flow while maintaining the magnetic field uniformity. (c) Top view of straight flow channel. Two adapters are adhered on either end of the flow channel creating a pressure-retaining joint. The external plates are shorter in length in order to promote the seal between the microscope slides and the adapter. (d) Top view of the expansion and contraction flow channels. The side walls in the larger width section are aluminum. The channel dimensions (in *mm*) shown in the figure are utilized in all flow channels unless otherwise noted.

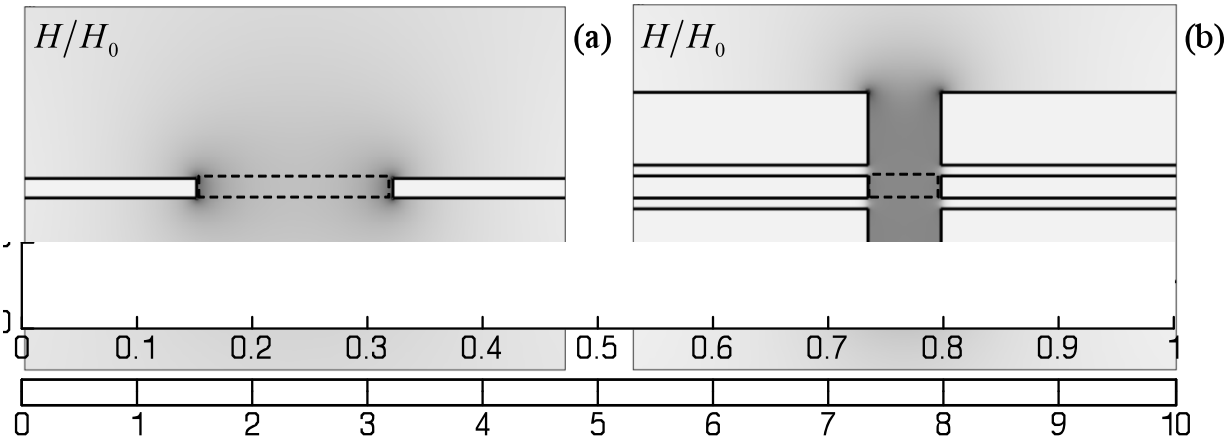

Figure 2: 2D magnetostatic finite element model for evaluation of field uniformity in the microchannels. Contours plotted for a zoomed section of the model to show the important features. (a) Without the external plates there is focusing of the field at the channel walls that would produce an undesirable magnetophoretic force on the particles. (b) The field uniformity in the microfluidic channel (shown by dashed lines) can be significantly improved with the addition of external plates.

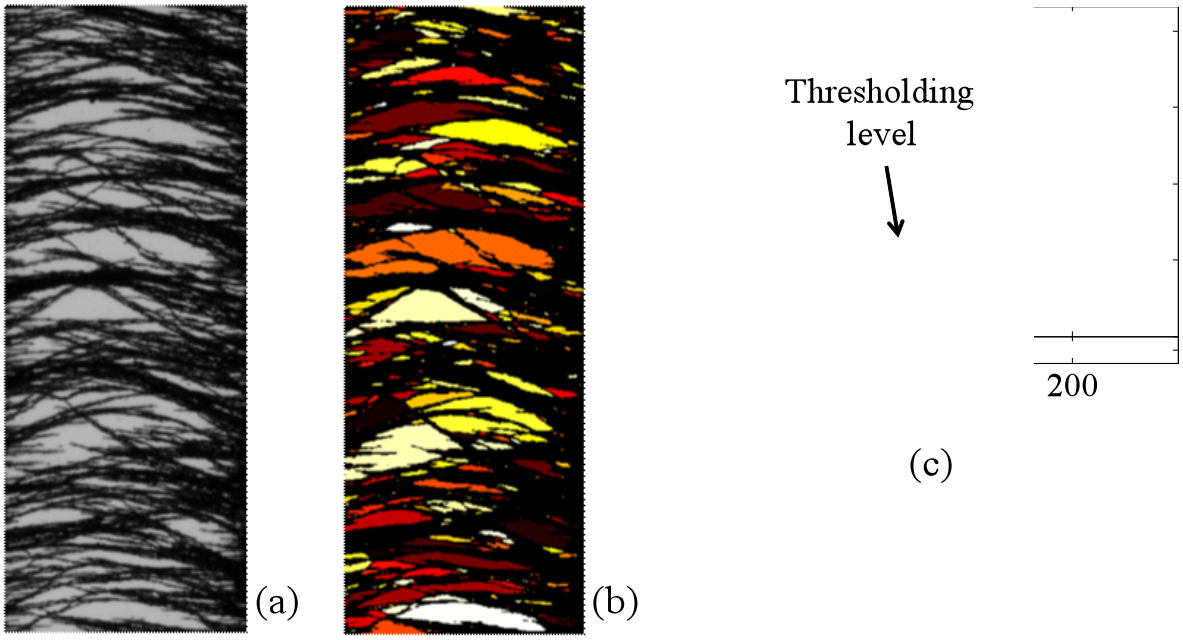

Figure 3: Image processing conducted to identify void clusters. (a) Original image captured at $Mn = 1.6 \times 10^{-3}$ in a rectilinear flow channel with the dimensions $w = 1.2mm$, $h = 0.3mm$. Flow is from bottom to top. (b) The image is converted into a black-and-white image using thresholding and processed with a cluster identification algorithm. The clusters are illustrated with a randomized coloring scheme. (c) The image consists of a bimodal distribution of pixels as seen in the histogram. Thresholding applied at the local minimum of the distribution, as indicated, effectively distinguishes between particles and voids.

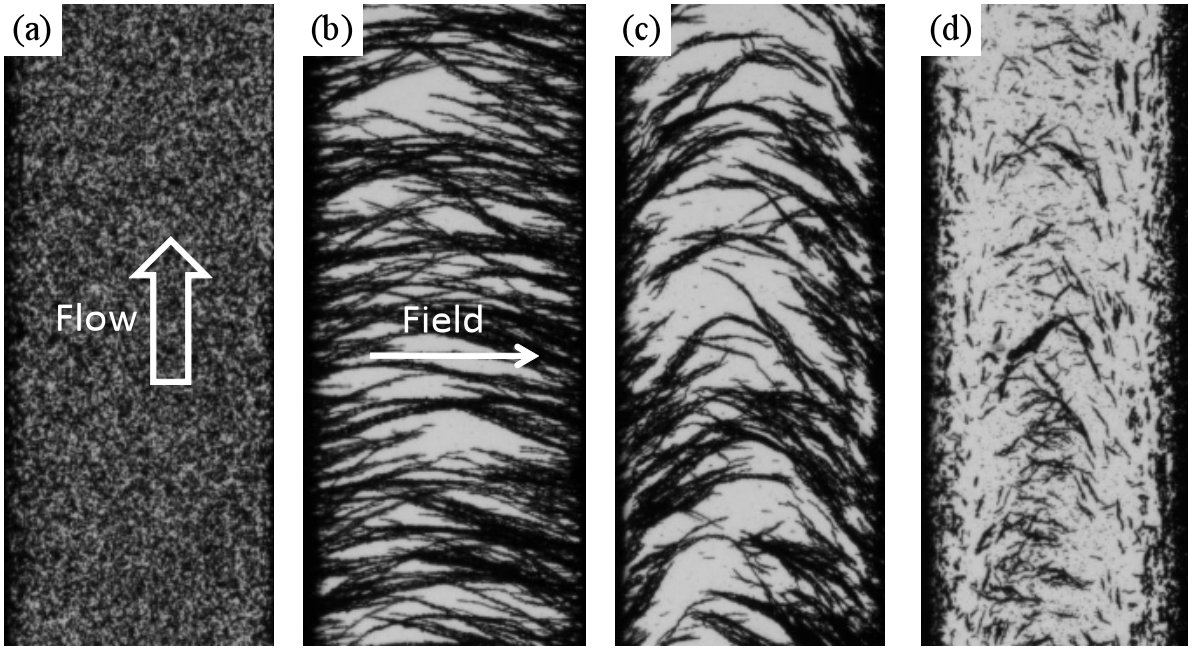

Figure 4: Aggregation and disaggregation of MR fluid flow in a ferromagnetic microchannel ($w = 1.2mm$, $h = 0.3mm$) during a typical experiment cycle. Flow is in the upward direction and the applied field is in the horizontal orientation. (a) Flow in a demagnetized channel without applied field. $Q = 10\,\mu l/min$ corresponding to a bulk velocity of $V_b = 4.6\times10^{-4}\,m/s$ and a Reynolds number $\mathrm{Re}_w = 1.4\times10^{-4}$. (b) Aggregated chain structures with $Mn = 6.3\times10^{-4}$. (c) Evolution of microstructure $t = 7s$ after field turned off. There is a layer of particles that are magnetically adhered to each channel wall. The dashed lines indicate the effective channel width w_{eff} in this flow regime. (d) After demagnetizing field has been applied.

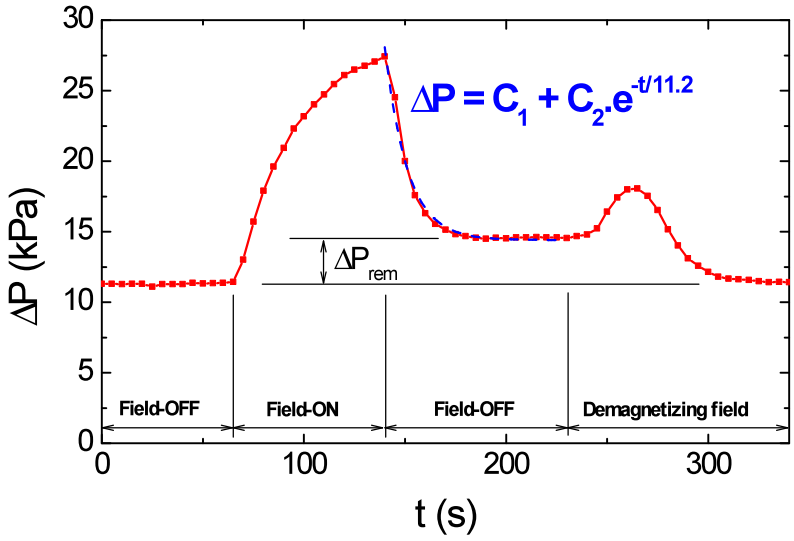

Figure 5: Differential pressure measured across the flow channel during a typical experiment in a rectilinear flow channel with the dimensions $w = 0.35mm$, $h = 1.2mm$. The dashed line is an exponential decay curve fitted to the field-off region of the curve. After the removal of the magnetic field, the pressure drop does not reduce to its original value, ΔP_0. This is caused by the particle-rich layer shown in Figure 4c. Using Equation (10), we can represent the new flow resistance in terms of an effective channel width $w_{eff}^{w \ll h} = 0.92$.

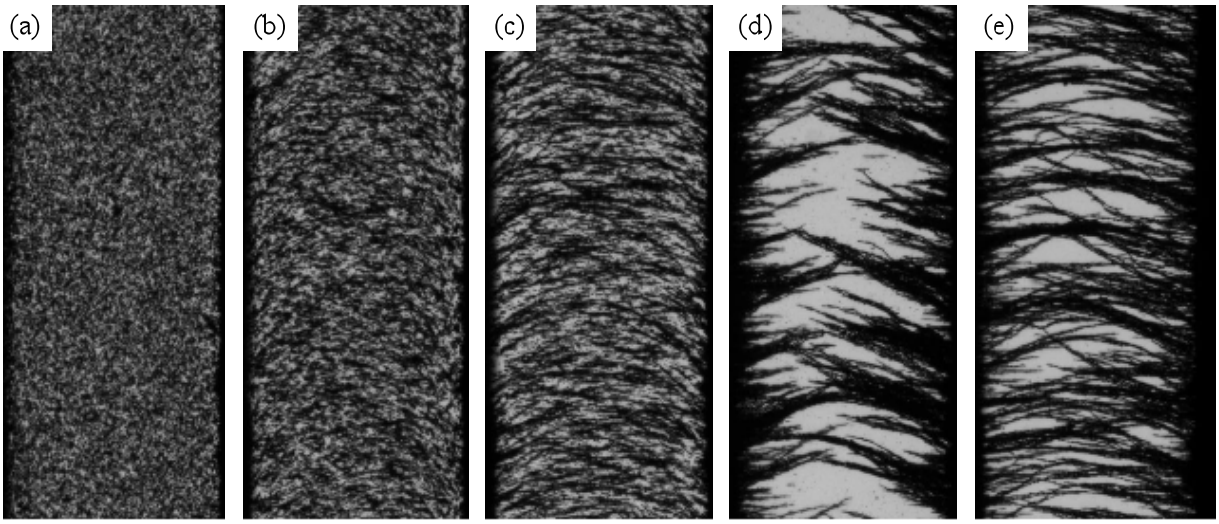

Figure 6: Evolution in aggregate microstructure of MR fluid flow. The Mason numbers in the images are (a) ∞ (field-off), (b) 0.16, (c) 0.018, (d) 0.0016 and (e) 0.00034. The channel dimensions are $w = 1.2mm$, $h = 0.3mm$.

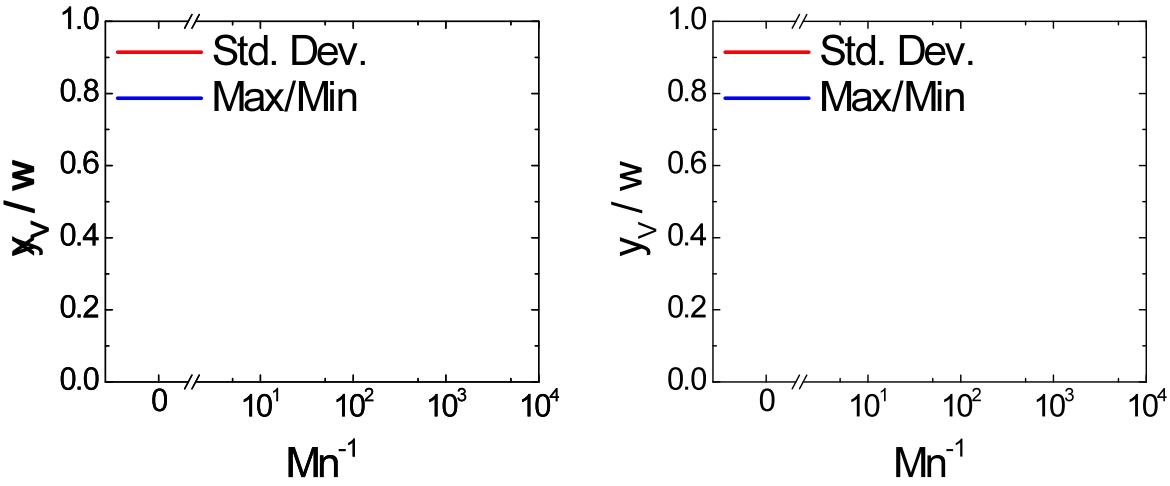

Figure 7: Horizontal and vertical void extents versus Mn^{-1} as identified by the cluster detection algorithm. The extents of a void in the horizontal, x_V and vertical, y_V, directions are equal to the respective side of the smallest upright rectangle that can completely cover the void. In the plots the mean (diamond symbols), standard deviation (red horizontal bars closer to the mean) and the maximum & minimum (blue bars) of the extents are plotted. The maximum void size is achieved for $Mn = 1.6 \times 10^{-3}$.

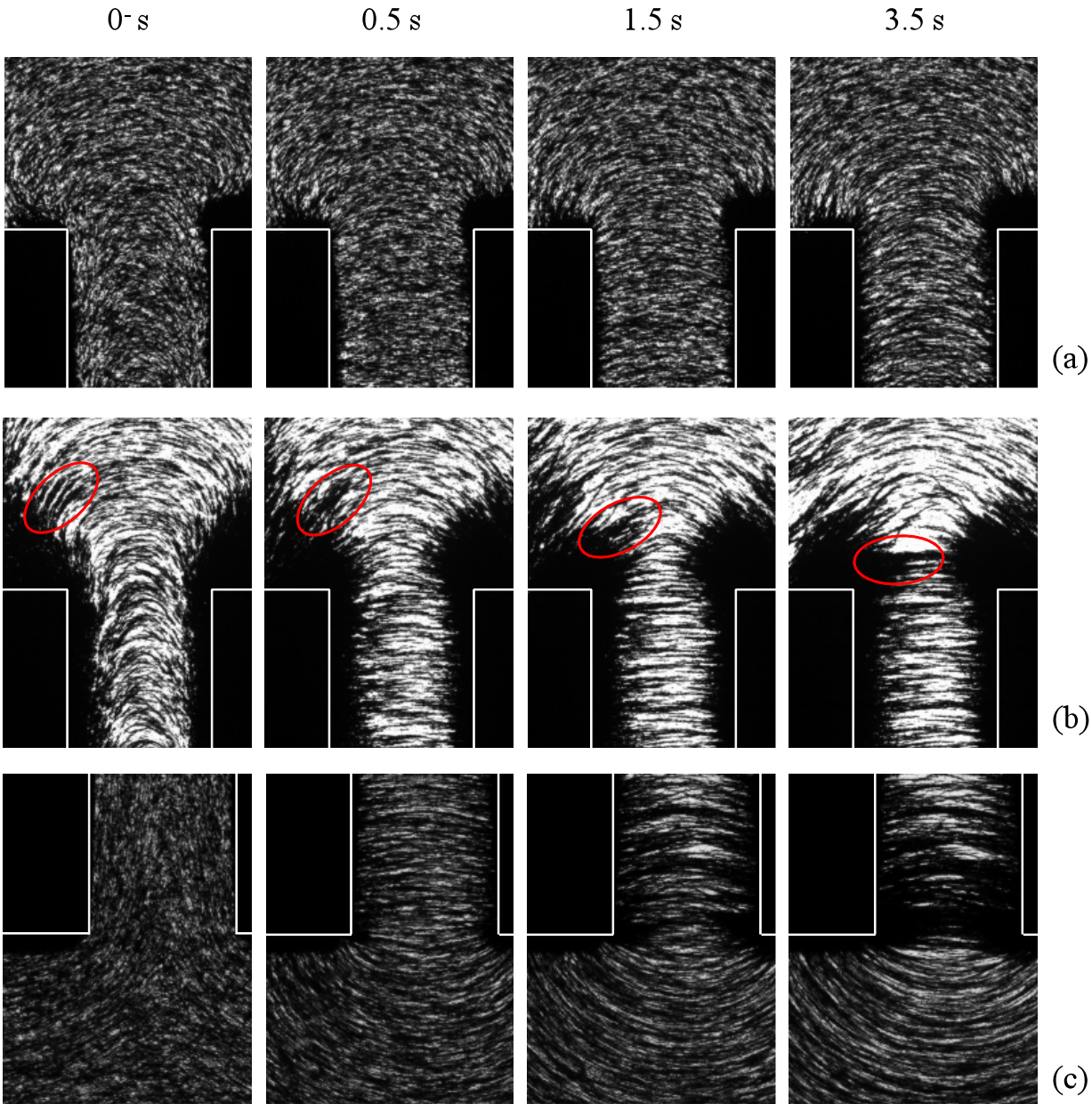

Figure 8: Contraction and expansion flow of MR fluid (width ratio, $w_1/w_2 = 3$). Square wave magnetic field with a rapid demagnetization cycle field-off state. The rectilinear section dimensions are $w_2 = 1.2mm$, $h = 0.3mm$. The field is turned on at time $t = 0$. (a) Expansion flow at $Mn = 3.8\times10^{-3}$, $\Psi \approx -0.011$. (b) Expansion flow at $Mn = 3.4\times10^{-4}$, $\Psi \approx -0.12$. (c) Contraction flow at $Mn = 3.2\times10^{-3}$, $\Psi \approx 0.012$. The magnetophoretic force caused by the field

gradient in the expansion flow channel at lower levels of $\Psi_d = -0.1$, as observed in (b), is large enough to reverse the flow of particles clusters back into the narrow channel. This can be seen by following the cluster of particles indicated with the red ellipse.